Characterization of a set of ECN Spray A injectors : nozzle to nozzle variations and effect on spray characteristics

2013-24-0037
Published 09/08/2013

doi:10.4271/2013-24-0037
saeeng.saejournals.org

Characterization of a Set of ECN Spray A Injectors: Nozzle to Nozzle Variations and Effect on Spray Characteristics

Louis-Marie Malbec
IFP Energies Nouvelles

Julio Egúsquiza
Pontifical Catholic University of Rio de

Gilles Bruneaux
IFP Energies Nouvelles

Maarten Meijer
TU/e

ABSTRACT

The Engine Combustion Network (ECN) is becoming a leading group concerning the experimental and computational analysis of Engine combustion. In order to establish a coherent database for model validation, all the institutions participating to the experimental effort carry out experiments at well-defined standard conditions (in particular at Spray A conditions: 22.8kg/m3, 900K, 0% and 15% O2) and with Diesel injectors having the same specifications. Due to the rising number of ECN participants and also to unavoidable damages, additional injectors are required. This raises the question of injector's characteristics reproducibility and of the appropriate method to introduce such new injectors in the ECN network.

In order to investigate this issue, a set of 8 new injectors with identical nominal Spray A specification were purchased and 4 of them were characterized using ECN standard diagnostics. In particular, the measurements include the nozzle hole diameter, the rate of injection, the liquid and vapor penetrations, the auto-ignition delay and the lift-off length. Variations of ambient temperature, oxygen concentration and density have also been performed.

In general the results show similar behavior to ECN standard injectors, confirming that this set of new injectors can be integrated into the pool of ECN injectors. However, discrepancies between spray characteristics were observed, although the injector specifications and the boundary conditions were sensibly the same. The sources of variations from injector to injector are analyzed in order to provide new information on the reproducibility of injectors characteristics, and improve the comparison methodology between experimental data and simulation.

CITATION: Malbec, L., Egúsquiza, J., Bruneaux, G., and Meijer, M., "Characterization of a Set of ECN Spray A Injectors: Nozzle to Nozzle Variations and Effect on Spray Characteristics," *SAE Int. J. Engines* 6(3):2013, doi:10.4271/2013-24-0037.

INTRODUCTION

The Engine Combustion Network (ECN) is a group of several laboratories around the world aiming at building a comprehensive experimental database for the validation of 3D models of gasoline and Diesel combustion. Standard experimental conditions have been defined ([1, 2]), that all the participating institutions have to precisely characterize and control prior to perform specific experiment. Concerning Diesel combustion investigations, the boundary conditions corresponding to the reference Spray A are described in Table 1.

The validation of the control of the boundary conditions is achieved in 2 steps:

- a direct measurement of the boundary conditions (ambient temperature and density, fuel temperature);
- a characterization of the behavior of the Diesel spray issued from one of the 5 single hole ECN injectors, supplied by Bosch, in the Spray A standard conditions, and using the

standard diagnostics defined by the network. Since the ECN injectors are similar, or to be more precise, the difference between the injectors is well know, differences in the spray behavior from one institution to another can provide information on possible differences in boundary conditions. This characterization is thus sensed to give a more precise insight into the degree of accuracy on the targeting of the boundary conditions.

Table 1. Description of ECN Spray A boundary conditions

Ambient gas temperature	900 K
Ambient gas pressure	near 6.0 MPa
Ambient gas density	22.8 kg/m^3
Ambient gas oxygen (by volume)	15% O_2 (reacting); 0% O_2 (non-reacting)
Ambient gas velocity	Near-quiescent, less than 1 m/s
Fuel injection pressure	150 MPa
Fuel	n-dodecane
Fuel temperature at nozzle	363 K (90°C)
Injection duration	1.5 ms
Injection mass	~3.5 mg

Previous work has been carried out to compare the experimental results obtained by different institutions. This work has been published in several paper ([2, 3, 4, 5]) and was also discussed during the two ECN workshops ([1, 6, 7]). The analysis of the results has shown that, in a first order, most of the institutions managed to reach the standard ECN conditions. But slight dispersion were observed between the results issuing from different institutions. This can be due to uncertainties in the thermodynamic boundary conditions. But an in-deep analysis has also highlighted that there are some dispersion in the injectors characteristics that can cause such differences. In spite of important efforts to precisely characterize the real specification of the ECN injectors and to relate them to the spray behavior, it is still difficulty to clearly identify the causes of the dispersion in the experimental results. This question is of major importance for model validation. Indeed, differences between experimental and simulation results can have difference sources that need to be understood to evaluate the models: such differences can be due to inaccuracy in the model, but also to boundary conditions uncertainties or injector to injector dispersion. Understanding the sources of these differences is therefore required to accurately determine the actual gap between the model and the experimental results. It is therefore one of the major concern of the ECN.

A second concern is linked with the hardware availability, which may become a major issue for the ECN mechanics. Indeed, ECN is a growing community, and more injectors are required to satisfy the demand. Solutions have to be found to face this situation. In this context, IFPEN has bought a new set of 8 single hole nozzles, with the same specifications as the ECN pool, hence called hereafter “Spray A.2 injectors”. These injectors have been bought in 2 pools of 4 injectors. The first pool has a part number of 102, and the second pool has a part number of 201. For each pool, the injectors are numbered between 01 and 04. The denomination of Spray A. 2 injectors is thus the following: the second injector of the first pool is for example named “Injector 102.02”. Then a characterization of a selection of four of these new nozzles was carried out to compare them with the standard ECN ones in terms of nozzle hole diameter, mass flow rate, liquid length, vapor penetration, auto-ignition delay and lift off length. Since the IFPEN apparatus has already been able to reach the target Spray A standard conditions it was relevant for this institution to perform such a characterization of the new set of injectors, before stating whether these injectors can be added or not to the pool of standard ECN injectors.

In addition, the novelty of the work presented in this paper is that a set of nominally identical injectors is compared in the same apparatus, hence in similar conditions. In previous ECN characterizations, the injectors were compared in different apparatus assuming that the differences from injector to injector was negligible or could be explained. In the present study, it is relevant to assume that the boundary conditions are identical, and that the differences observed in the experimental results are mainly caused by dispersion in the injectors characteristics. This characterization will therefore help to understand how differences between nominally identical injectors can affect the main characteristics of the spray. The characterization of these Spray A.2 injectors thus meets the two concerns described earlier.

EXPERIMENTAL APPARATUS

Combustion vessel

IFPEN uses a preburn constant volume vessel to perform the spray analysis. Its characteristics are presented in Figure 1 and Table 2. The vessel operation has already been extensively described in previous work ([8, 2]), it is only briefly summarized here.

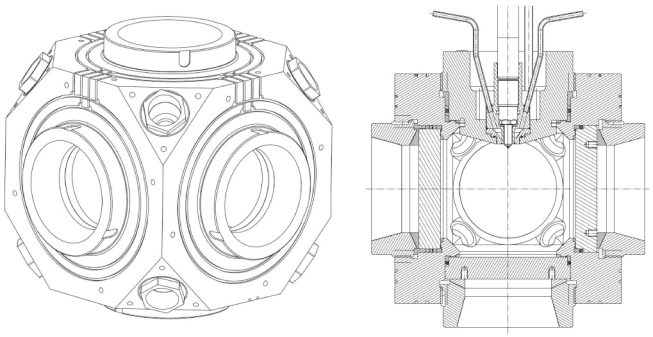

Figure 1. Global view (left) and sectional drawing (right, with an injector in vertical position) of the IFPEN vessel.

Table 2. Characteristics of the IFPEN constant volume Vessel

Internal width	125 mm
Windows diameter	80 mm
Internal volume	1400 cm^3
Ignition system	4 spark plugs, in the lower corners
Wall temperature	473 K (200°C)
Nozzle tip protrusion	3 mm

In a preburn constant volume vessel, the fuel is injected in a chamber whose pressure, density and temperature are representative of the thermodynamical conditions encountered in the combustion chamber of a real engine at the injection timing. This requires the ability to reach high temperatures and density, which is achieved by the combustion of a flammable mixture. The different steps of this process are listed below:

Filling: The vessel is sequentially filled with the flammable mixture, composed of hydrogen (H_2), acetylene (C_2H_4), nitrogen (N_2) and oxygen (O_2). The pressure and temperature of the mixture at the end of the filling process defines its density. The proportions of the gases are controlled by their partial pressures when introduced in the vessel. The proportions between N_2 and O_2 are set in order to obtain the desired O_2 fraction after the preburn event.

Preburn (or precombustion): The mixture is mixed with a stirrer during 30 seconds after the end of the filling, before the flammable mixture is ignited by 4 spark plugs located in the corners of the vessel. The combustion of the mixture generates a rapid rise of the pressure and temperature within the vessel.

Cool down: After the preburn, the pressure and temperature slowly decrease due to heat losses.

Injection: When the desired temperature is reached, the injection is triggered and the diagnostics are performed.

Two preburn vessels are available at IFPEN, with identical characteristics and control system. Previous ECN campaigns ([2, 9, 4, 3]) were carried out on the first vessel. The current experiments were carried out on the second vessel. The first vessel is therefore well characterized to reach ECN conditions, but the second one, although identical, has not been checked for ECN targeting. One additional objective of the boundary conditions characterization was therefore to verify that similar conditions are obtained in this second vessel.

Injection system

The fuel is supplied to the injector through a pipe linked to a common rail, respecting the ECN specifications ([2]). A hydro-pneumatic pump is used to generate the pressure. Its maximum capacity is 2750 bars. A set of 8 nozzles, consisting in 2 series of 4, have been bought from Bosch. These nozzles are nominally identical to the ECN standard injectors and are mounted on commercial CRI 2.16 bodies. The nominal characteristics of these nozzles are described in Table 3. In order to differentiate the new injectors against the standard ECN ones, they are named Spray A.2 (instead of Spray A for the original ECN injectors).

Table 3. Nominal characteristics of ECN nozzles

Nozzle outlet diameter	90 µm
Nozzle shaping	Hydro-eroded
Nozzle K factor	1.5
Mini-sac volume	0.2 mm^3
Discharge coefficient C_d	0.86

Previous characterizations of standard ECN nozzles, whose results are summed-up in Table 4, have highlighted some dispersion compared to the nominal characteristics ([5]). Therefore, dispersion is also expected for the Spray A.2 injectors, which needs to be quantified.

Table 4. Summary of ECN nozzles geometry measurements ([5])

Injector #	Outlet diam. [µm]	Inlet diam. [µm]	Nozzle length [µm]	K-factor -
Nominal	90.0	105	-	1.5
Uncertainty	1.0	2	5	0.3
210675	89.4	116	1030	1.3
210677	83.7	116	1026	1.8
210678	88.6	117	1044	1.8
210679	84.1	116	1026	1.8

MEASUREMENT TECHNIQUES

The measurement techniques that have been used can be divided into two categories: characterization of the boundary conditions, and characterization of the sprays. These characterizations have been carried out in standard ECN conditions, described in Table 1.

Characterization of Boundary Conditions

All these techniques aim at providing an exhaustive characterization of all the parameters that can have an effect on the spray behavior.

Nozzle geometry

A *FEI quanta 600 F* Scanning Electron Microscope (*SEM*) has been used to define the geometry of the nozzle exit hole. The main advantage of this microscope over conventional optic devices is the increased magnification possibilities using electrons instead of light. In this case, the sample is scanned with a focused primary beam of electrons, which will interact with the specimen. Subsequently, the amount of electrons released by the interaction on a certain spot, determine the amplitude of the signal using a specific detector.

Rate of injection

The mass flow rate was measured with a commercial EMI2-EFS rate meter. The measurement principle is the following: the fuel is injected in a chamber filled with fuel. The volume of this chamber is controlled by a moving piston. A back pressure is applied to this piston. The piston displacement is measured and is used to provide the mass flow rate.

Nozzle tip temperature

The evolution of the fuel temperature during the injection event is likely to influence the spray characteristics, in particular the liquid length. Therefore it is important to be able to control its temperature. Since the measurement of the fuel temperature during the injection event is a challenge, the solution chosen by the ECN community is to measure the evolution of the temperature in the sac volume during the preburn using a dummy injector ([6, 4]), therefore without fuel and without injection. The nozzle has no orifice, and the injector is equipped with a type K thermocouple which allows to measure the temperature in the sac volume, at different distances from the bottom of the sac (Figure 2).

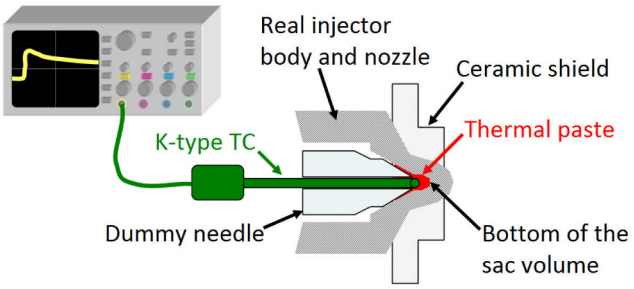

Figure 2. Scheme of the setup used to measure the temperature in the sac volume with a dummy injector

In order to limit the temperature rise within the sac volume, ECN injectors are shielded with a ceramic cover (or ceramic shield) that insulates the nozzle and reduces the heat transfers between the hot gases within the vessel and the injector. The dummy injector is also mounted with the same ceramic shield (Figure 2).

Ambient temperature

After the preburn event, during the cool down process, the temperature and the density are not homogeneous in the vessel. Average values (named as "bulk") are thus different from local values, especially in the center of the vessel (named as "core"). The standard conditions specified by ECN are for the core values, which are thus the ones that must be controlled.

The two vessels are permanently equipped with pressure sensors. This means that for all preburn events, the bulk temperature T_{bulk} (i.e the average temperature) in the vessel can be computed through the perfect gas law:

$$T_{bulk} = \frac{P_{vessel}}{Z.r.\rho_{bulk}} \qquad (1.1)$$

where Z and r are respectively the compressibility factor (needs to be taken into account for real gas effects) and the gas constant of the mixture, P_{vessel} is the pressure measured by the sensor, and ρ_{bulk} is the average density in the vessel, controlled during the filling of the vessel. Because of the thermal boundary layer generated by heat transfers at the walls of the vessel, the core temperature T_{core} (in the center of the vessel) is higher than the bulk temperature T_{bulk}. Consequently, since the pressure P_{vessel} is homogeneous in the vessel, there is also a density gradient. Based on the perfect gas law, we have:

$$\rho_{core}.T_{core} = \rho_{bulk}.T_{bulk} \qquad (1.2)$$

Since there are 2 unknown values, T_{core} and ρ_{core}, another relation is required. This is the aim of the ambient temperature measurements. The temperature within the vessel is measured with a type K 50µm diameter thermocouple. The temperature is measured in the center of the vessel. The raw temperature measured by the thermocouple is corrected to take into account the effects of the radiations, convection, and thermocouple inertia ([2]). The characterizations of the temperature distribution within the first IFPEN vessel have been carried out previously ([2, 9]). The temperature distribution in the second vessel, used in the present work, is supposed to be identical.

Spray Characterization

After the characterization of the boundary conditions, the second step aims at characterizing the behavior of the spray for the different injectors.

Liquid length

Several techniques can be used to measure the liquid penetration of a spray. Pickett et al. ([10]) have performed an exhaustive study of these different techniques. Among them, the ECN participants agreed to chose the Diffuser Back-Illumination (DBI) technique, because it is simple, quantitative and robust. The advantages and limitations of this DBI method are detailed in ([10, 9]) but can be summarized as: 1) it is quite simple to set up, 2) it is self-calibrated 3) it enables robust quantitative *comparisons* between results of several institutions, 4) it suffers from beam-steering, which limits the measurement precision for the actual liquid length. But this limitation is not a major issue if the objective is to compare results obtained between institutions, since in this case the comparison of the signal drop off is enough. The corresponding setup is presented in Figure 3.

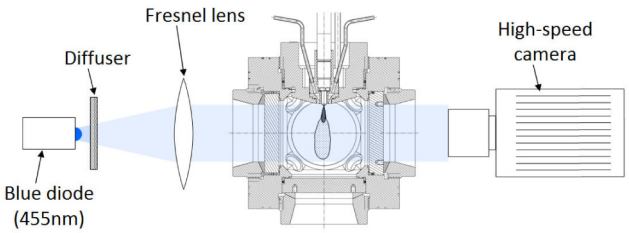

Figure 3. Diffuser back-illumination setup

The light source is a blue diode at 455nm. In order to obtain an illumination as homogeneous as possible, an engineered diffuser is place just in front of the diode. A Fresnel lens is then used to collimate the light rays. The signal is collected by a high-speed Photron SA1 camera, whose frame rate is 120kHz, equipped with a 50mm f/1.2 lens and a 8mm extension ring. The resolution of the images is 320×112pxls, and the spatial scale is 88.5µm/pxl. The resulting field of view is about 28×10mm^2. An example of the images obtained with such a technique is shown in Figure 4, together with the corresponding time averaged image during the injection event.

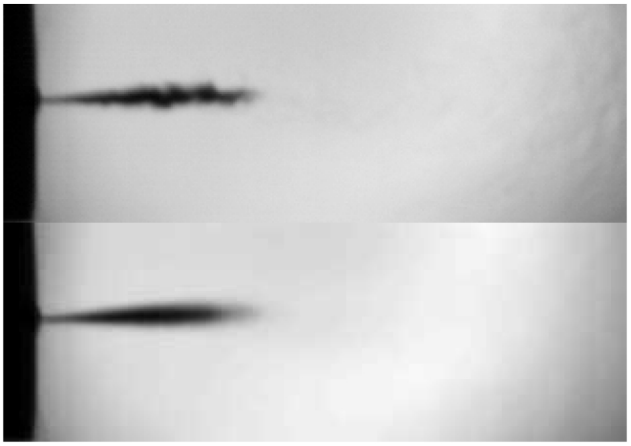

Figure 4. Example of an image obtained with the DBI setup (top), and the corresponding time averaged image during the steady state of the injection event (bottom)

The processing method consists in converting the time averaged intensity images into extinction images. The extinction is noted τ and is computed as:

$$\tau = -\ln\left(\frac{I}{I_0}\right) \qquad (1.3)$$

where I is the image intensity, and I_0 is the reference intensity (i.e. without any extinction). Then, the extinction profile along the spray axis is analyzed. An example of such a profile is displayed in Figure 5.

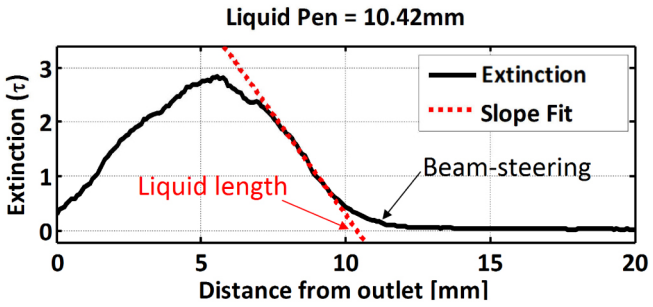

Figure 5. Example of the processing of extinction images

Near the liquid core tip, beam-steering is significant, and thus the extinction value is the consequence of both the light extinction and the beam-steering. The profile in this region can therefore not be taken into account to compute the liquid length. Instead, the slope of the decay of the extinction profile is computed, and the liquid length is defined as its intersection with the x-axis.

Vapor penetration

Measurement of the vapor penetration is performed with a Schlieren setup, detailed in Figure 6.

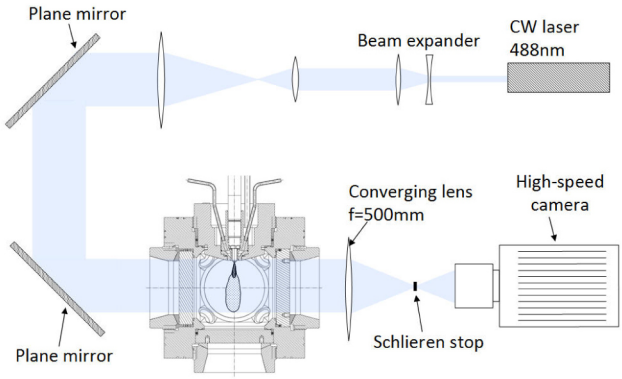

Figure 6. Schlieren setup

The light source is a continuous wave laser at 488nm. The beam issuing from the laser is shaped into a larger parallel beam of 8cm diameter. The light is collected with a high-speed Photron SA1 camera, equipped with a 100mm f/2.8 lens and a 8mm extension ring. The resolution of the images is 640×240pxls, and the spatial scale is 117µm/mm. The resulting field of view is 7.5cm × 2.8cm. The frame rate is 30kHz. The spatial filter (Schlieren stop) is a cutoff disk whose diameter is 1.2cm, that blocks non-deviated rays. As a result the sprays appears in white on a dark background (dark field Schlieren). This setup has been chosen against the bright field setup because it gave the best contrast for the spray images. An example of such an image is given in Figure 7.

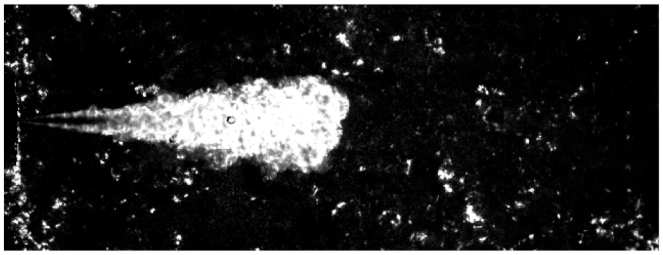

Figure 7. Example of an image obtained with the Schlieren setup

The processing of such images consist of detecting the border of the spray and then taking the maximum value of vapor penetration at each timing.

Auto-ignition

The detection of the auto-ignition was performed by two different methods. The first one is based on direct visualization of the flame chemiluminescence with a high-speed camera. For this method, a trade-off has to be made between time resolution and sensitivity. Indeed, the higher the frame rate, the higher the precision of the auto-ignition delay determination. But at the same time, increasing the frame rate will decrease the integration time of the camera, and thus decrease the amount of light collected, hence the auto-ignition detection sensitivity. In the present study, a compromise frame rate of 40kHz was chosen, corresponding to a 25µs precision on the auto-ignition delay measurement. To optimize the sensitivity of the setup to chemiluminescence, the camera was equipped with a high aperture 50mm f/1.2 lens. Such a setup is sensitive enough to detect the light emission from the cool flame. The difficulty of the image analysis is therefore to identify the contribution of high-temperature chemiluminescence versus cool flame. The methodology used in the present work is based on an intensity threshold: below this threshold, the light emission was considered as being due to the cool flame; above, it is a attributed to the high temperature combustion. This methodology is described in [3]. In our study, we obtained 8-bits images for which the leveling-off value representing high temperature chemiluminescence was approximately 100 counts. The threshold for auto-ignition delay detection was thus 50 counts. When the saturation of the camera sensor is observed, this is attributed to the soot incandescence. Based on this distinctions, we have considered the following analysis of the intensity I:

- background noise: $0 \leq I \leq 2$ counts
- cool flame: $3 \leq I \leq 49$ counts
- high-T combustion: $50 \leq I \leq 254$ counts
- soot: $I = 255$ counts

Figure 8 displays an example of the temporal evolution of the high speed combustion images. Cool flame zones are displayed in blue, high-temperature combustion in orange, and soot in red. When the high-temperature combustion has started, the blue zones can no longer be considered as cool flame. The auto-ignition delay is defined as the time when the first occurrence of high-temperature chemiluminescence (orange) is observed (t=0 corresponds to the effective start of injection).

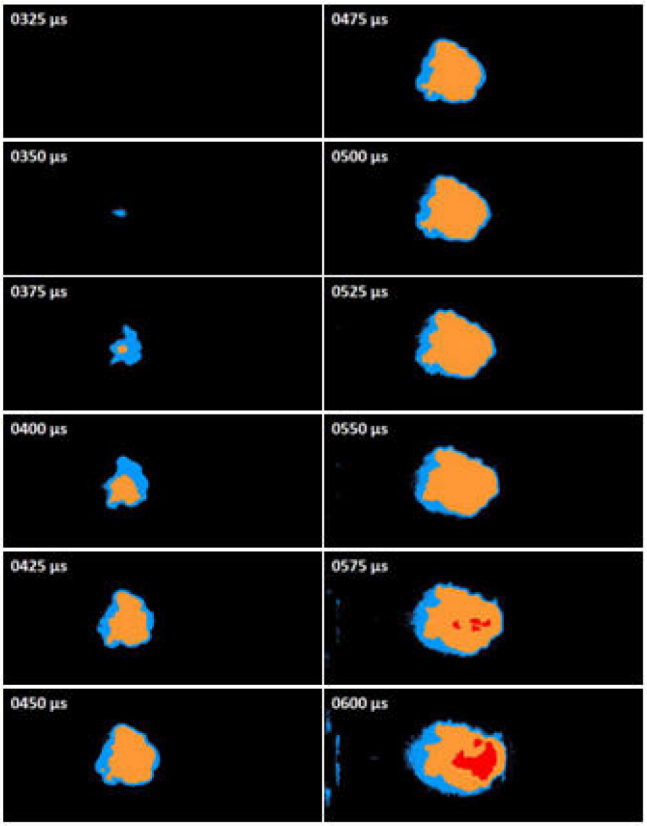

Figure 8. Temporal evolution of the combustion. Images obtained by direct visualisation of the combustion. Injector is on the left side and injects towards the right. Spray A conditions: 22.8kg/m^3, 900K, 15%O_2 (%vol.).

The second method used to measure auto-ignition delay is based on the analysis of the pressure evolution in the vessel. The latter was equipped with an additional pressure sensor to the one used to record the preburn event, dedicated exclusively to the measurement of the pressure rise during the combustion of the injected fuel. This pressure sensor is located in one of the lower corners of the vessel, thus requiring to remove one of the 4 spark plugs. An example of the signal obtained with this pressure sensor is presented in Figure 9, showing that the signal is quite smooth before the start of combustion, and becomes more noisy afterwards. The processing consists in detecting the time of the first peak of the noise (red circle on Figure 9 - bottom)

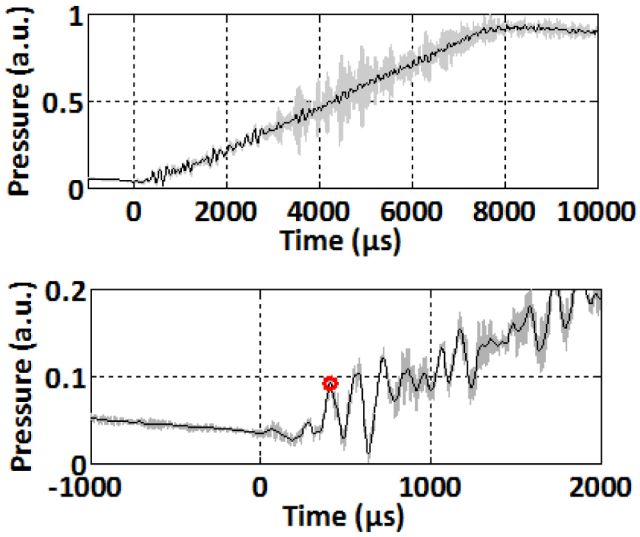

Figure 9. Example of pressure signal obtained with the dedicated pressure sensor during the spray combustion. Raw signal is in light gray, filtered signal in black. The bottom figure is a zoom of the top one. The ignition timing is represented by a red circle.

Indeed, the pressure sensor is located approximately at a distance L=10cm from the auto-ignition sites. The pressure wave thus reaches the sensor after a delay noted t_{sound} determined by:

$$t_{sound} = \frac{L}{c} = L \cdot \sqrt{\frac{\rho_{core}}{\gamma . P_{vessel}}} \qquad (1.4)$$

where c is the speed of sound. In spray A conditions (P=60bar, ρ_{core}=22.8kg/m3) and assuming that γ=1.4, t_{sound} is approximately 165µs.

Lift-off length

The measurement of the lift-off length was performed through the collection of the emission of the excited OH* radical at 310nm, which is a marker of high temperature diffusion flames ([11]). This method has been recommended by Higgins and Siebers ([12]) and is since widely used. The setup is presented in Figure 10.

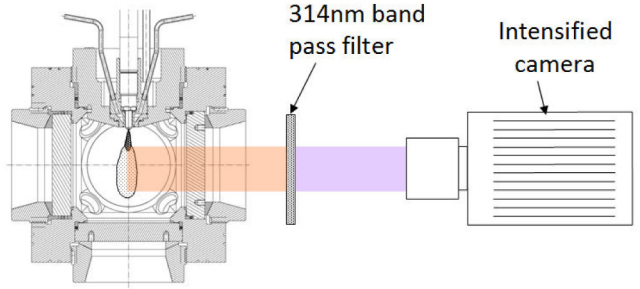

Figure 10. Chemiluminescence OH* setup

The light emission from the flame is filtered with a 314nm +/− 15.38nm band-pass filter and a 358nm low-pass filter, and is then collected with a intensified Princeton camera, equipped with a 45mm f/1.8 UV lens and a 8mm extension ring. The resulting spatial scale is 163µm/pxl. The injection duration has been extended in order to obtain a longer steady state period for the diffusive combustion process. This allows a longer opening time for the intensified camera, and thus a better chip averaged image. The duration of the electric command is 5795µs (instead of 795µs for Spray A), and the signal is collected during the steady-state portion of the combustion, between 2ms and 5ms after the electric command of the injector.

The processing method is described in [13, 1], and is explained in Figure 11. On the top of this figure, an example of an image of OH* chemiluminescence is presented. The injector's orifice is located on the left, at the coordinates [0;0]. Two lobes of more intense chemiluminescence appear on the image, and the intensity profiles parallel to the spray axis and crossing those two lobes are plotted on the bottom of Figure 11. A reference intensity is defined by the average of the first local maximum intensities along the two profiles. This reference intensity is plotted in dashed blue line. The lift-off length is defined as the distance between the orifice and the location of the first occurrence of an intensity higher than half of the reference intensity.

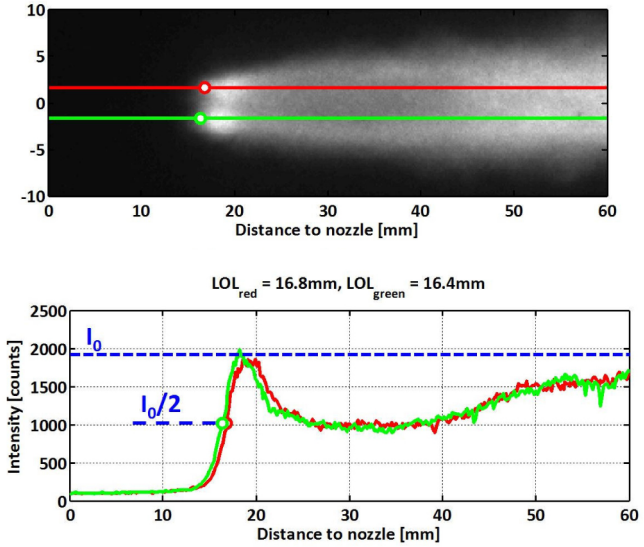

Figure 11. Example of an image of OH* chemiluminescence (top) and of the associated processing (bottom).

For each image, 2 values of lift-off length are found, and for each functioning point, 5 images are acquired, which gives a total of 10 values. The average value and standard deviation of the lift-off length are computed on these 10 values.

RESULTS

Boundary Conditions

Fuel temperature

Figure 12 displays the temperature measurements performed with the dummy injector during steady-state condition (prior to the preburn) and during preburn and cool down events. The reference time (t=0) corresponds to the electric command of the spark plugs. For these measurements, the thermocouple is positioned within the sac volume of the dummy injector at 4 different positions relative to the bottom of the sac volume (0, 1, 2 and 3 mm). During the steady-state condition, the initial temperature was regulated to the target value (90°C for Spray A conditions) at the reference position (0 mm). In this figure, the dashed lines correspond to standard deviation, which is lower than ±0.5 °C.

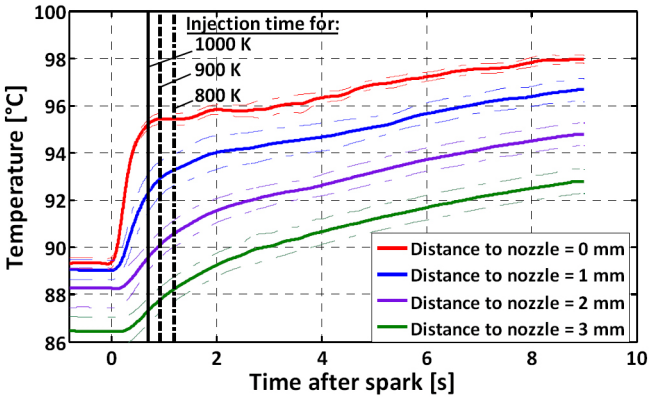

Figure 12. Measured fuel temperature traces at different locations inside the injector nozzle. 15% O2 combustion products.

First looking at the steady state behavior, the results show that the temperature varies within the sac volume. Before preburn, while at 0mm the temperature is 89.5°C, close to the target 90°C, the temperature decreases slightly when measured deeper into the sac volume (89.1°C, 88.3°C and 86.5°C at 1, 2 and 3 mm respectively).

Figure 13 presents an example of an x-ray tomography image for injector 678 ([5]). It appears that the sac is about 1mm deep. If the needle position during the opening is added (500µm at full lift, see [5]), it gives a depth of approx. 1.5mm. Therefore, a distance of 3mm to the bottom of the sac volume is higher than the depth of the sac itself, and the thermocouple is not in the sac anymore. However, the volume of injected fuel for Spray A conditions (3.5mg, i.e. app. 4.5mm^3) is higher than the sac volume (0.2mm^3), so that the injected fuel is not initially completely contained in the sac volume. These measurements show that a temperature gradient exists within the injector, that can affect the injected fuel temperature.

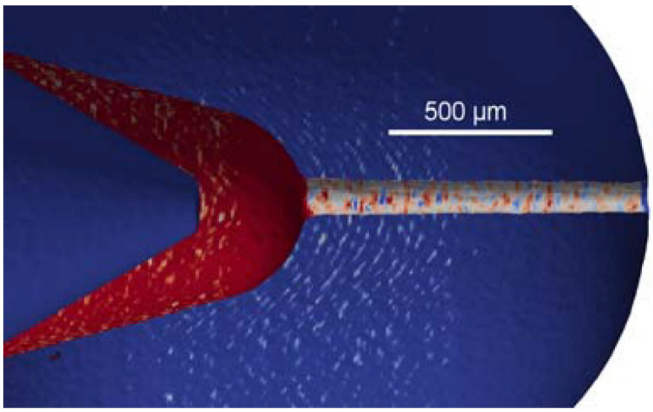

Figure 13. X-ray tomography image obtained for the injector 678. Image presented in [5].

During preburn and cool down, the nozzle tip temperature increases due to heat transfer from the hot gases inside the vessel. Black vertical lines in Figure 12 indicate the injection timing for 3 ambient gas temperature conditions (800, 900 and 1000 K) at 22.73 kg/m^3 mean core density, showing that the temperature at the bottom of the sac volume of the dummy injector (distance of 0 mm) is around 95 °C for the 3 conditions at the injection timing, corresponding to a 5°C increase due to preburn. Also, the temperature rise is less pronounced deeper in the nozzle (it rises only by about 1°C at the 3mm position). In addition, these results show that the ceramic shield is efficient to limit the increase of the nozzle tip temperature. Indeed, similar measurements without the ceramic shield showed significantly higher temperature increase [2].

After dismounting the dummy injector, it was observed that the thermal paste located in the sac volume had dried out. Additional measurement are necessary to assess the effect of this issue on the nozzle tip temperature measurements.

Ambient temperature and density

The experiments presented in this paper were carried out in the second IFPEN vessel. While most of the ECN experiments were carried out in the first one ([2, 4, 9, 3]), recent ECN experiments in this second vessel ([14]) have shown that although the two vessels are identical, different conditions were obtained between the two vessels. The source of these differences is investigated here.

Figure 14 shows the initial ambient temperature, i.e. the temperature just before the preburn event, in the two vessels, measured by a thermocouple for a number of experiments. The results show that the initial temperature in the second vessel is 28K higher than in the first vessel.

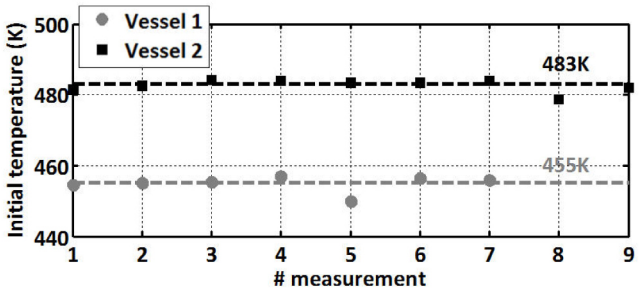

Figure 14. Comparison between the initial temperatures of the 2 IFPEN vessel

The most probable explanation for this difference is the closed-loop control of the temperature of the walls of the vessels. Indeed, the walls are heated at a target temperature of 473K by heating resistances. A thermocouple is inserted within the vessels' walls to measure the wall temperature and is used as input parameter for the control loop. The results show that the implantation of this control thermocouple is not exactly identical between the two vessels, so that different initial temperatures are observed. If not taken into account, this difference generates a significant error in the targeting of ambient conditions ([14]). Being well characterized in the present experiments, this difference is taken into account in the targeting of ECN spray A conditions. Also, a more robust implantation system for the control thermocouple was designed at IFPEN in order to ensure similar operation between the two vessel, and will be used for future ECN experiments.

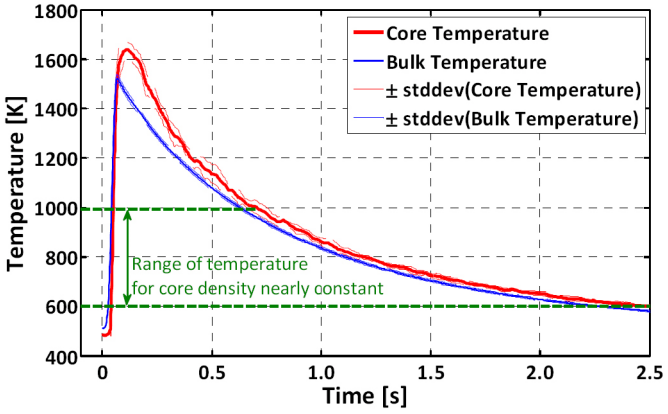

Figure 15. Measured gas temperature during the premixed burn and cool-down period. 15% O_2 combustion products, 23.49 kg/m^3 mean bulk density.

Once the initial core temperature issue addressed, the evolution of the ambient core temperature during the precombustion and the cool down processes have been characterized. Figure 15 presents the ensemble averages of the core and bulk temperatures, for 9 precombustion events with a bulk density of 23.5kg/m^3 and and an oxygen concentration of 15% (%vol.). The results show that, as expected, the core temperature is higher than the bulk.

From the core temperature, the core density can be deduced with the perfect gas law:

$$\rho_{core} = \frac{P_{vessel}}{r.Z.T_{core}} \qquad (1.5)$$

The ensemble average core density is shown in Figure 16. The core density appears to be constant during a large temporal period (between around 0.6 and 2.5s after spark timing). Referring to Figure 14, this temporal range corresponds to 600K<T_{core}<1000K, which is the range of interest for the present work. Within this range, the following relationship between core and bulk density is used:

$$\rho_{core} = c.\rho_{bulk} \qquad (1.6)$$

where c is constant and equal to 0.968 in the present measurements. This relationship, in addition to formulas (1.1) and (1.2) allows to compute the core density and temperature directly from the pressure information. This relationship between core and bulk density is slightly different from the one proposed by Sandia ([15]):

$$\rho_{core} = c(T_{bulk}).\rho_{bulk} \qquad (1.7)$$

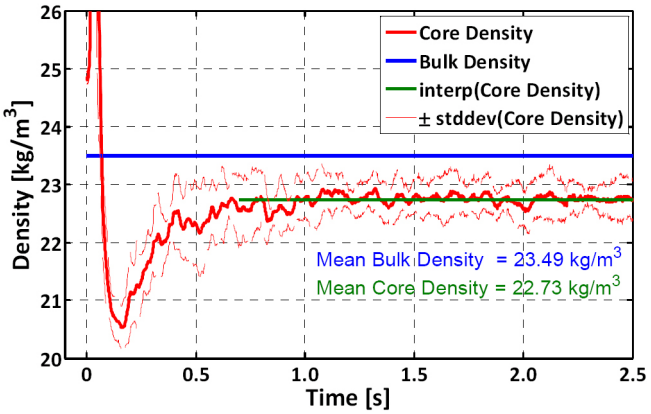

Figure 16. Average core gas density in the center of the vessel. 15% O_2 combustion products, 23.49 kg/m^3 mean bulk density and 22.73 kg/m^3 mean core density.

The proportionality coefficient c is not constant in this case, it varies with the bulk temperature ([15, 2]). One explanation for this difference might be the difference in mixing fan speed between the apparatus of the two institutions, generating different boundary layer thicknesses, hence different bulk to core relations. Further investigations are required to confirm this hypothesis, such as boundary layer characterization by thermocouples.

The formula (1.6) is valid for a bulk density of 23.5kg/m^3. But ECN conditions include core density variations, down to

a value of 15.2kg/m^3. Therefore, additional measurements were performed with a bulk density targeting this lower value. Based on formula (1.6), the bulk density should be:

$$\rho_{bulk} = \frac{1}{c}\rho_{core} = \frac{1}{0.968}\cdot 15.2 = 15.7 \text{ kg/m}^3 \quad (1.8)$$

The corresponding results are shown in Figure 17 for the evolution of core and bulk temperature, and Figure 18 for the evolution of core and bulk density. Again, it is found that the core density is constant during a wide temporal range. Nevertheless, the ratio between the core and bulk densities is smaller, close to 0.99. This result seems to show that the temperature and density gradients within the vessel are decreasing when the bulk density decreases. This might be explained by the fact that at lower density, the thermal boundary layers are thinner. Again investigations of the thermal boundary layer thicknesses are required to confirm this hypothesis. This result must be taken into account when variations of core density are carried out.

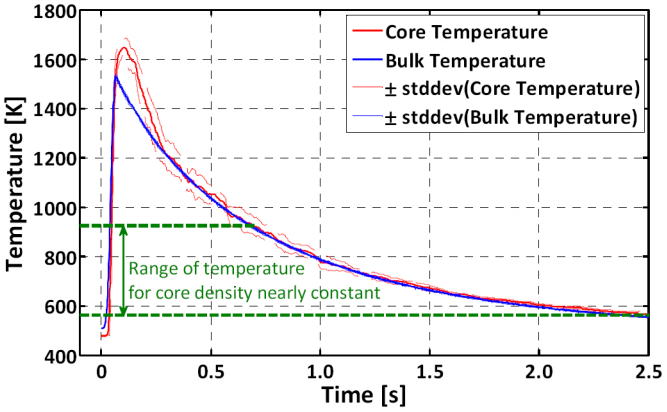

Figure 17. Measured gas temperature during the premixed burn and cool-down period. 15% O_2 combustion products, 15.68 kg/m^3 mean bulk density.

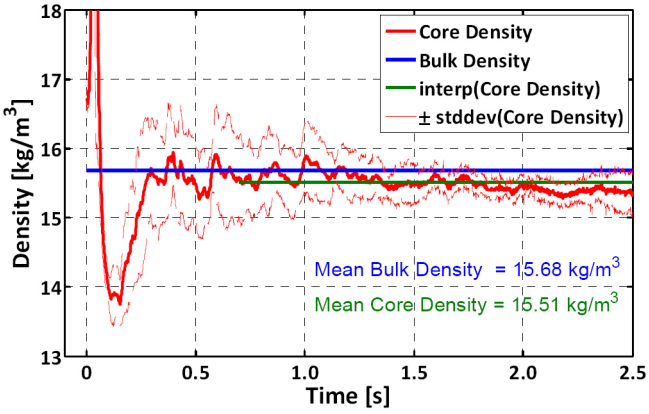

Figure 18. Average core gas density in front of injector. 15% O_2 combustion products, 15.68 kg/m^3 mean bulk density and 15.51 kg/m^3 mean core density.

Injectors Characterization

The characterization of the Spray A.2 injectors requires that Spray A boundary conditions have been reached. Therefore, in the analysis of the experimental results, the first step will be to compare the results obtained with the injector 678 to previous results obtained by different institutions. This comparison should allow to conclude whether the Spray A conditions have been targeted or not. Then, in a second step, the behaviors of Spray A.2 injectors will be compared to injector 678. The same methodology will be used for the analysis of all the experimental results.

Injector nozzle geometry

The images obtained from the SEM scanner are used to analyze the nozzle geometry for the 8 different injectors. Conclusions are made about the inner nozzle surface, based on the direct view, holding the nozzle under an angle of 30 degrees inside the scanner. An example of the images obtained is presented in Figure 19. For each batch (2 times 4 nozzles), it is observed that the first specimen shows a smoother inner nozzle surface than the last one. This effect of production is shown in Figure 19, where the image on the left is the first and the image in the middle is the last injector nozzle from one batch. It is hard to conclude whether the imperfections are pollutants or material imperfections or both.

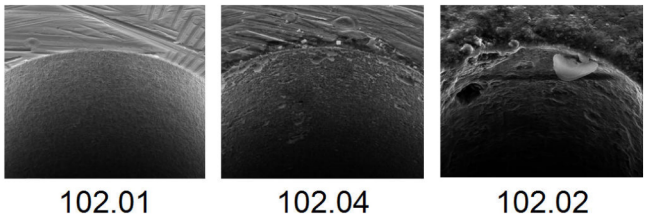

Figure 19. SEM images of the inner nozzle surface roughness. Showing the effect of production (left vs. middle) and aging (left vs right).

Aging effect is defined as the alteration of the orifice surface because of its use (several preburn and injection events). The aging effect is shown in the right image from Figure 19. An important observation is that the aging of the nozzles has a more severe impact on the inner nozzle surface roughness than the dispersion caused by production. This particular nozzle (102.02) has been used for approximately 100 runs inside the preburn vessel during earlier measurement campaign. Because of the aging it has been decided not to use this particular nozzle in this work. Nevertheless, the images do show the need to keep track of aging effect for all ECN injectors.

One must keep in mind that such significant aging effect might not be relevant for all ECN apparatus. Indeed, the IFPEN preburn vessels are using a gas mixture that generates high amounts of water vapor in the combustion products, therefore enhancing possible condensation effects hence rusting issues. Because of this issue, IFPEN is considering a

change of its preburn gas mixture composition in order to minimize the vapor content of the products formed during the preburn event.

Knowing the nozzle exit diameter for each injector is important for a direct comparison and to explain the observed differences in measurement results in the preburn vessel. The processing method is imaged in Figure 20. The diameter of each nozzle is determined from a perfect circle minimizing geometric error (sum of squared distances from the points to the fitted circle) using nonlinear least squares (Gauss Newton). This circle is plotted in dashed red line in Figure 20, top right. From the obtained results, it is concluded that the perfect circle assumption does not fit the real injector hole dimensions as desired. The nozzle exit holes are, in line with the original ECN injectors, all slightly elliptical. Therefore a second optimization routine is written where fitting is performed by nonlinear least squares, optimizing the squared sum of orthogonal distances from the points to the fitted ellipse (dashed green line in Figure 20). The normalized surface area, defined as the calculated surface divided by the surface for a nominal 90 µm injector is also presented. From Figure 20, it can be concluded that the different injectors do not differ much. The (blue) encircled injectors are used for the presented work in this paper. The effect of aging on the nozzle hole surface (injector 102.02) is clearly shown.

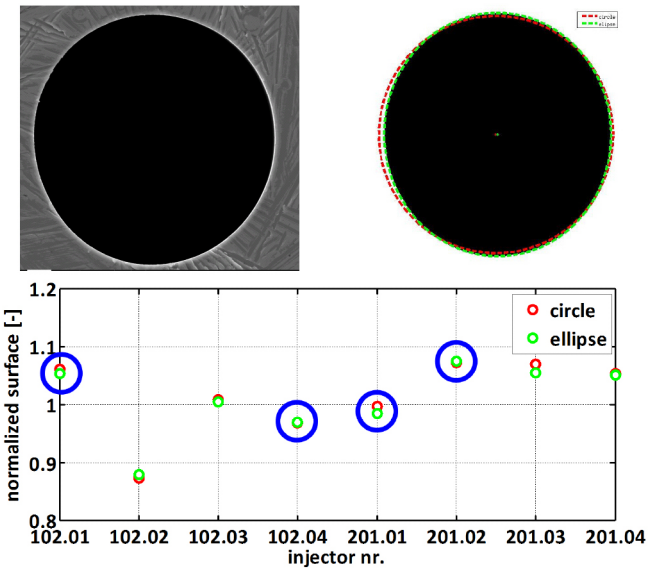

Figure 20. Approach to calculate the nozzle exit hole surface area. Starting from the raw SEM image (upper left), fitting a perfect circle and ellipse (upper right) and the obtained results compared to the nominal injector area (based on a diameter of 90mm).

Rate of injection

The first analysis of the rate of injection results consists in verifying that the measurement methodology of IFPEN was consistent with CMT measurements of the rate of injection, that were so far the only available ones, in order to ensure consistent measurements within the ECN. For this validation, the rates of injection obtained at IFPEN and at CMT with injector 678 are compared, and the results are presented in Figure 21. The measurements at IFPEN are performed with the EMI2-EFS while at CMT an injection rate meter based on the Bosch anechoic tube is used. Moreover, low pass filtering is required to post process the signal issuing from the EMI2-EFS. Therefore direct comparison of the mass flow rate results obtained from the two institutions with different equipment and post processing is not straightforward. However, the comparison shows that with respect to opening and closing phases, both profiles shows similar behavior. Also the mass flow rate level obtained during the steady state period is very close. This figure therefore shows that the EMI2-EFS device used at IFPEN gives similar results in terms of mass flow rate level to the Bosch tube used at CMT.

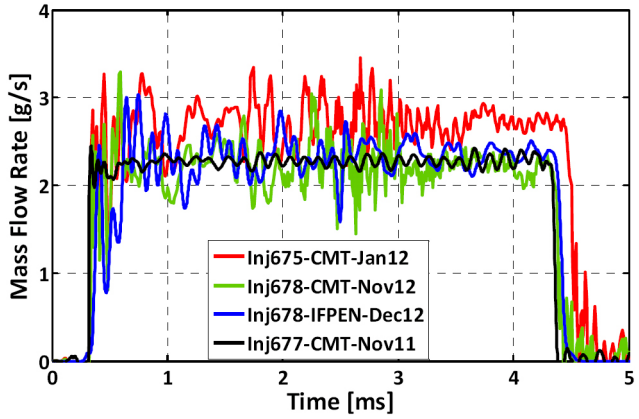

Figure 21. Mass flow rate for injectors 675, 677 and 678, measurements from IFPEN (average of 100 injections) and CMT. Experimental conditions: 2.5 ms energizing time, 1500 bar injection pressure and 60 bar back pressure.

A second level of analysis consists in analyzing the behavior of the injector 678. For this purpose, the rate of injection of injector 678 is compared to other standard ECN injectors, 675 and 677. Injector 675 is chosen because its characteristics have been less altered than other standard ECN injectors. Besides, injector 677 has been used by Sandia during the first experimental characterization campaign ([2]). Injection mass flow rate curves for the standard ECN injectors 675, 677 and 678 are compared in Figure 21.

The observation of Figure 21 leads to the following remarks:

• The mass flow rate of injector 677 is lower than injector 675. This indicates that there is dispersion in the mass flow rates of standard ECN injectors. In [5], such a dispersion has already been reported.

• The mass flow rate of injector 678 is similar to 677. However, the steady state mass flow rate for injector 678 was about 2.5g/s in [5], whereas it is only about 2.2g/s on the last

measurements shown in Figure 21. This reduction might be explained by a damage of the injector nozzle surface since the nozzle tip appears rusty. Further investigation of the internal surface of 678 has been carried out within the ECN to analyze this change in mass flow rate with time. The results of these characterization will be shown in future references. They confirm an aging effect on the inner surface of the nozzle hole.

Finally, the behaviors of Spray A.2 injectors (102.01, 102.04, 201.01 and 201.02) are compared to Spray A ones, and more precisely to the injectors 675 and 677. The results are presented in Figure 22. First, we can observe that very similar mass flow rates are obtained for all the Spray A.2 injectors.

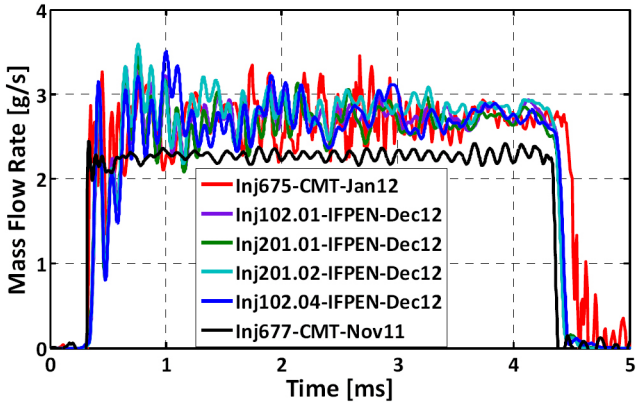

Figure 22. Mass flow rates of Spray A.2 injectors compared to 675. Experimental conditions: 2.5 ms energizing time, 1500 bar injection pressure and 60 bar backpressure.

This is further confirmed by the time-averaged values of the steady state mass flow rates (average between 2 and 3ms) for spray A.2 injectors, presented in Table 5.

Table 5. Time-averaged values of the mass flow rate during the steady state period

Injector	Steady-state mass flow rate (g/s)
102.01	2.77
102.04	2.77
201.01	2.73
201.02	2.85

Besides, injector 675 and Spray A.2 injectors have also similar rates of injection, higher than injector 677. These results show that the mass flow rates of Spray A.2 injectors are very similar to the standard of ECN Spray A. This statement must now be confirmed by analyzing the behavior of the corresponding sprays.

Spray Characterizations

Based on the characterization of the boundary conditions, the spray A target has been reached. The characterization of the behaviors of injectors can thus be carried out. In the previous part, injector 675 was considered concerning the mass flow rates measurements. But a complete set of data concerning the spray behavior is not available for this injector. Therefore, for this part, the results of injector 678 and Spray A.2 injectors will be compared only to injector 677, which has been characterized by Sandia ([2]).

Liquid length

Liquid length measurements of the 678 nozzle were performed at IFPEN in two different vessels (1 and 2) and at three different time period (December 2009 and April 2012 for measurements performed in vessel 1, and December 2012 for measurements performed in vessel 2). 677 characterization was performed at Sandia.

Figure 23 displays the liquid length as a function of the ambient gas temperature for injectors 678 and 677. The results show relatively good agreement at 900K, although obtained in different institutions, different vessels and in different time periods. The dispersion that can be observed is within the standard deviation of the measure (±0.45 mm). Besides, the liquid length decreases with increasing ambient temperature as expected ([16]).

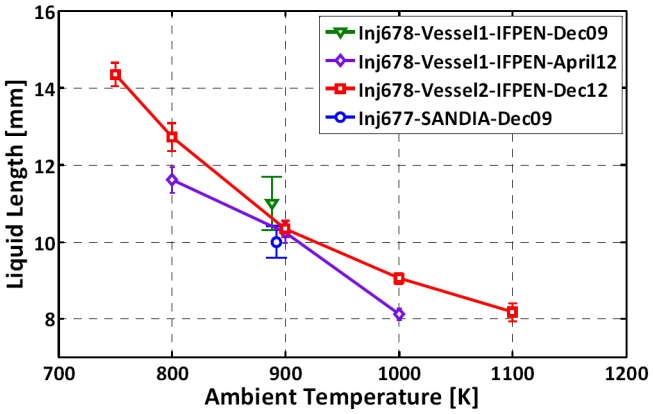

Figure 23. Influence of ambient temperature on liquid length ECN Injectors 678 and 677 at IFPEN and Sandia. Experimental conditions: 22.8kg/m^3, 0% ambient oxygen, fuel at 363 K and 1500 bar injection pressure.

Figure 24 displays the liquid length as function of ambient temperature for the 4 Spray A.2 injectors and compared to injector 678. Significant differences in liquid length can be observed. The longest liquid lengths were obtained for injector 201.02, and the shortest for injector 678.

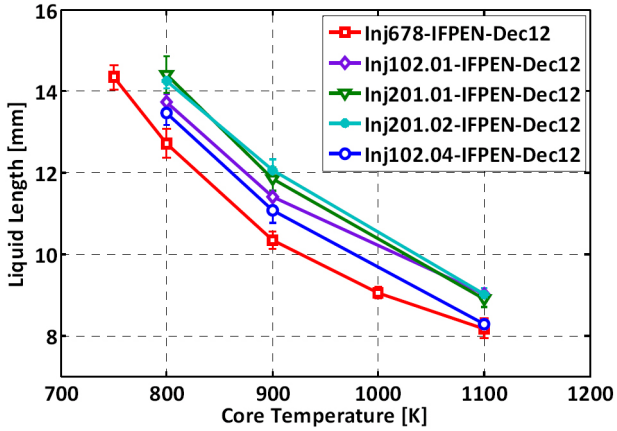

Figure 24. Influence of ambient temperature on liquid length for Spray A.2 injectors and injector 678. Experimental conditions: 22.8kg/m^3, 0% ambient oxygen, fuel at 363 K and 1500 bar injection pressure.

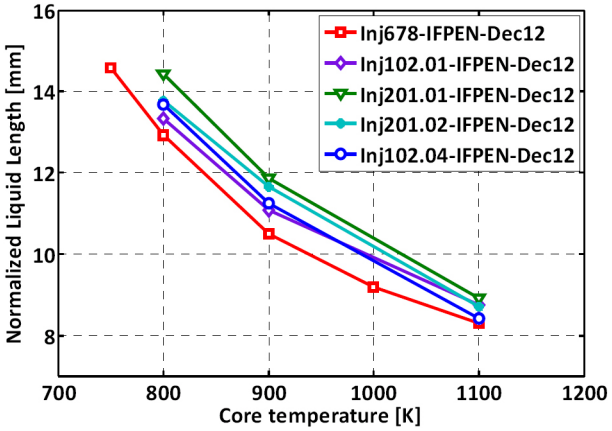

Figure 25. Effect of temperature on the liquid length normalized by the ratio between the nominal orifice diameter (90µm) and the measured one.

At a constant temperature of 900K, representing Spray A conditions, a 1.72 mm span is obtained between injectors 678 and 201.02. This difference results in an increase in liquid length of about 17%. One cause that could explain this dispersion in the measured liquid lengths are the variations in the nozzle exit diameters. Siebers ([17]) has proposed a formula to compute the liquid length:

$$LL = \frac{b}{a} \cdot \sqrt{\frac{\rho_f}{\rho_a}} \cdot \frac{\sqrt{C_a} \cdot d}{\tan(\theta/2)} \sqrt{\left(\frac{2}{B(T_a, P_a, T_f)} \right)^2 - 1} \qquad (1.9)$$

where a and b are constants, ρ_f and ρ_a the densities of the fuel and ambient air, C_a is the area contraction coefficient, d is the orifice diameter, θ is the spray angle, and B(T_a,P_a,T_f) characterizes the evaporation of the fuel. Based on this formula, the liquid length is proportional to the orifice diameter d (supposing that the dependence of the spray angle to the diameter is neglected). Therefore, to analyze the contribution of nozzle diameter variations on the liquid length dispersion, it is convenient to normalize the liquid length by the orifice diameter. In the present work, it is normalized by the ratio of the nominal diameter (90µm) to the measured exit diameter $d_{measured}$ (1.10).

$$LL_{norm} = LL_{measured} \cdot \frac{90}{d_{measured}[\mu m]} \qquad (1.10)$$

LL_{norm} thus represents what would be the liquid length if the exit diameter of the injectors was exactly 90µm. The results are plotted on Figure 25, showing that although reduced from 17% to 13%, the dispersion still exists.

So, the dispersion observed on Figure 24 are only partially due to differences in the orifices diameters. Additional investigation of the internal geometry of the nozzle would be required to better understand the causes of the dispersion in liquid length between the different nozzles.

Vapor penetration

Figure 26 displays the vapor penetration as a function of time after the start of injection (ASI) for injector 678 and 677. Vapor penetration measurements of the nozzle 678 were performed at IFPEN in two different vessels and two different time period (april 2012 for measurements performed in vessel 1, and December 2012 for measurements performed in vessel 2). Vapor penetration measurements of the nozzle 677 were performed at Sandia. For the clarity of the figure, the standard deviation is not represented, but it is lower than ±3.2 mm for IFPEN results, and lower than ±4.0 mm for Sandia's results.

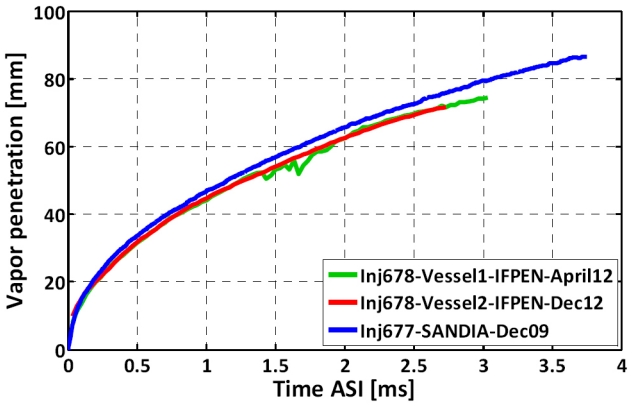

Figure 26. Comparison of vapor penetration for ECN injectors 678 and 677 at IFPEN and Sandia. Spray A conditions: 22.8kg/m^3, 0% ambient oxygen, fuel at 363 K and 1500 bar injection pressure.

The vapor penetrations of 678 obtained in the two IFPEN vessels are identical, showing that the experiment is repeatable within the two IFPEN apparatus and that same boundary conditions have been targeted on the second vessel. Also, as time ASI increases, the vapor penetration of 678 is significantly lower than 677.

It has been shown earlier in this paper that injectors 677 and 678 have similar mass flow rates. However, CMT has performed momentum measurements for both injectors, whose results are displayed in Table 6.

Table 6. Results of mass flow rate and momentum measurements obtained by CMT

	Nozzle 677 (November 2011)	Nozzle 678 (October 2012)
Momentum [N]	1.46	1.22
MFR [g/s]	2.27	2.25

It appears that, although the mass flow rates are very similar between the two injectors, the momentum is lower for injector 678. As exposed earlier in this paper, this might be explained by a degradation of the nozzle inner surface. This lower momentum for injector 678 might be the cause of the lower vapor penetration. In order to verify this hypothesis, a 0D model of Diesel spray was used ([15, 18]). This model requires the mass flow rate and the momentum of injectors as inputs. Based on the vapor penetration measurements from Sandia, the vapor angle θ_{spray} of the 677 spray was computed using the 0D spray model according to the methodology proposed in ([18]), giving θ_{spray} = 21.0°. The vapor penetration computed by the spray model with this angle is displayed in Figure 27. The same calculation was performed for injector 678 assuming that the spray angle is the same, hence assuming that differences in spray penetration between injectors 677 and 678 are only due to the difference in momentum. Therefore the vapor penetration of injector 678 was simulated with the 0D spray model with a spray angle θ_{spray} = 21.0°, and the mass flow rate and momentum displayed in Table 6. The result is displayed in Figure 27.

These results show that the simulated vapor penetrations are close to the measured ones. Moreover, the same differences in vapor penetration between injectors 677 and 678 are obtained with the simulation. This result therefore tends to show that lower momentum for injector 678 is the main reason to its lower vapor penetration than 677.

Figure 28 displays the vapor penetration evolution for the 4 Spray A.2 injectors, compared to 678. Overall, good agreement is observed. An insert is included in Figure 28 to zoom in on the different curves and show more details of the dispersion between the penetration curves. The variation span is about 2.3 mm at 1 ms ASI, corresponding to 5%. The dispersion between nozzles is therefore lower than the standard deviation, and also significantly lower than the dispersion observed in liquid length (which is around 17%). This result therefore seems to show that nozzle to nozzle differences have a lower effect on vapor penetration than on liquid length.

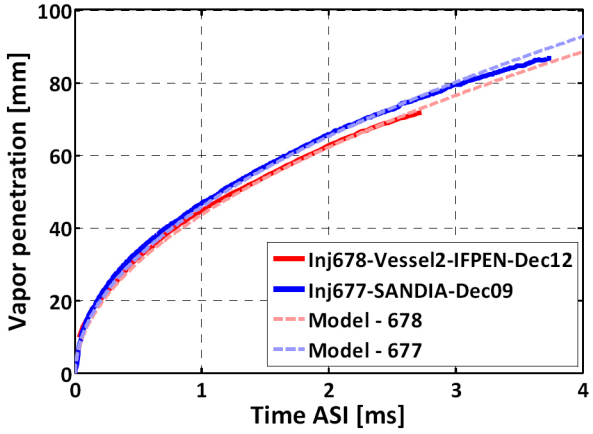

Figure 27. Comparison of measured vapor penetrations with the ones computed with the 0D spray model for injectors 677 and 678.

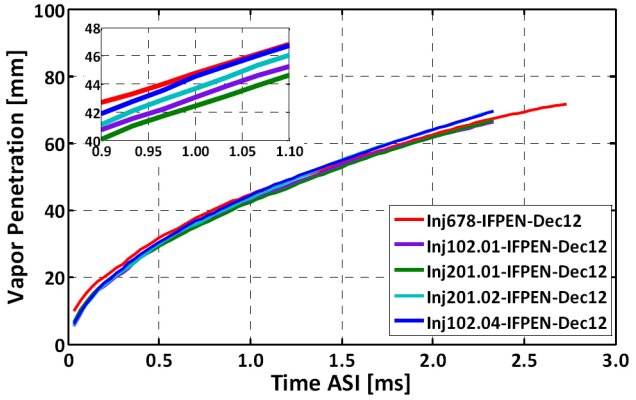

Figure 28. Comparison of maximum vapor penetration for ECN like injectors. Spray A conditions: 22.8kg/m^3, 0% ambient oxygen, fuel at 363K and 1500 bar injection pressure.

However, although small, some dispersion is observed in the vapor penetration. We analyze the cause in more detail here. This dispersion is not caused by the mass flow rates, since they are similar for all the Spray A.2 injectors. Besides, it has been shown than the lower penetration of injector 678 compared to injector 677 could be explained by the lower momentum of injector 678. Therefore, the same assumption can be used to explain the dispersion in the vapor penetration of Spray A.2 injectors. The 0D model of Diesel spray can be used to assess this dispersion in the momentum. The steady-state mass flow rates of all the Spray A.2 injectors are known (Table 5). If the assumption is made that the spray angles of the Spray A.2 injectors are equal to 21.0° (spray angle of injector 677), the input momentum can be tuned in order to match the vapor penetration. This gives a value of momentum

for each Spray A.2 injectors. These values are presented in Table 7.

Table 7. Values of the momentum of Spray A.2 injectors computed with the 0D model of Diesel spray.

Injector	Steady-state momentum (N)
102.01	1.19
102.04	1.36
201.01	1.17
201.02	1.35

It appears that, based on the methodology described above, there is a difference of about 14% between the higher and the lower momentum value. Momentum measurement would be helpful to confirm or not these results.

Auto-ignition

As presented in the measurement techniques section, the auto-ignition delay was determined either by detection of the luminosity of the high temperature combustion, either by the detection of the pressure rise. Variations of temperature and oxygen concentration have been performed for the different injectors. For all these variations, the auto-ignition delays based on the two different measurement techniques are compared in Figure 29.

The results show that the two methodologies give very similar results, therefore validating the 2 post-processing methods. Also, since the two methods give similar results, in the following, only the auto-ignition delays based on the pressure sensor analysis will be shown. Figure 30 displays a comparison of the results obtained with the 678 injector at IFPEN with results obtained with other ECN nozzles in different ECN institutions [7]. The results are very similar between institutions, and the dispersion is below the standard deviation at 900K (std. dev=28µs).

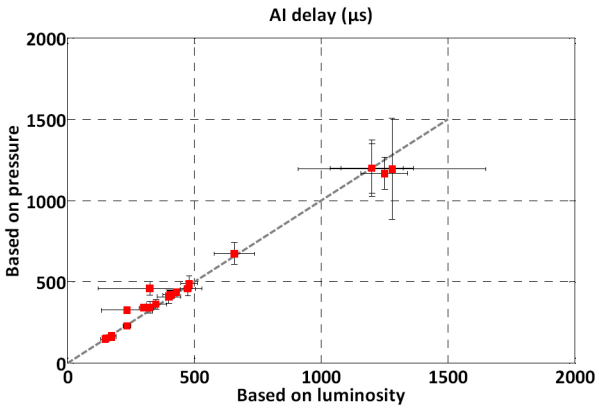

Figure 29. Comparison of the auto-ignition delays obtained with the luminosity and pressure methods

Figure 31 displays the evolution of auto-ignition delays for varying ambient temperature for 678 nozzle compared with 3 Spray A.2 nozzles. Figure 32 displays the same comparison for a variation of oxygen concentration. The difference from nozzle to nozzle is below the standard deviation therefore showing that all the nozzle give very similar results in terms of auto-ignition timing.

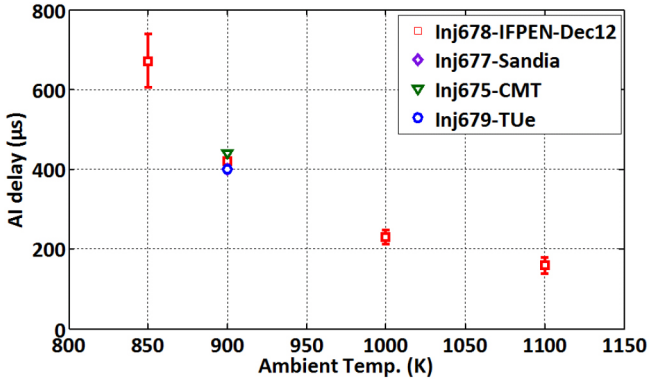

Figure 30. Comparison of the measured auto-ignition delays between several institutions, for varying ambient temperature. Conditions: 22.8kg/m3, 15%O_2 (%vol.)

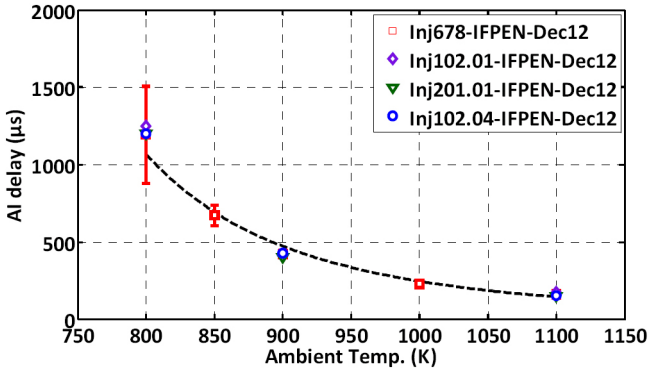

Figure 31. Dependence of the auto-ignition delay to temperature, for the different injectors tested. Conditions: 22.8kg/m^3, 15%O2 (%vol.)

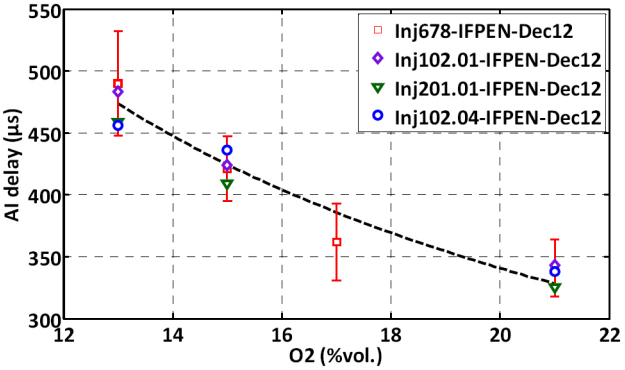

Figure 32. Dependence of the auto-ignition delay to oxygen concentration, for the different injectors tested. Conditions: 22.8kg/m^3, 900K.

The interest of such an analysis of the effect of varying ambient parameters (temperature, oxygen concentration) is to investigate the consistency of the results on a wide range of parametric variation, and therefore to provide a more robust comparison than a single condition analysis. It also minimizes the possibility to have similar results between injectors and institutions because of compensating errors. To compare the results of these parametric variations between institutions, it is convenient to use the correlations formula in order to reduce the comparison to a tendency analysis. Concerning the auto-ignition delay (AI), an Arrhenius law is commonly used to express the dependancy of this value to ambient temperature and oxygen concentration:

$$t_{AI} = A.e^{\frac{B}{T}}.[O_2]^C \qquad (1.11)$$

The values for B and C obtained with the present IFPEN results are given on Figure 31 and Figure 32 and are compared with the one obtained by Sandia and CMT in Table 3.

Table 8. Comparison of the dependance of auto-ignition delays to ambient temperature and oxygen concentration.

	B	C
Sandia *(SAE 2005-01-3843)*	6534	-0.96
CMT	6487	-1.22
IFPEN	5873	-0.76

The results show slight differences between the coefficients obtained by different institutions, but relatively small compared to the sensitivity of these coefficients For these three institutions, the same global tendencies are observed for variations of ambient temperature and oxygen concentration, therefore confirming the consistency of the results.

Lift-off length

The effects of ambient gas oxygen concentration on lift-off length are displayed in Figure 33 for nozzle 678 and three Spray A.2 injectors (102.01, 201.01 and 102.04) at the targeted 900K temperature. The oxygen concentration was varied from 21 % by volume to 13%. The standard deviation is lower than ±1.1 mm.

The results show as expected that for all the nozzles the lift-off length increases as the ambient gas oxygen concentration decreases ([19]). The variation from injector to injector is about 1.4 mm, *i.e.* slightly above the measurement standard deviation. Also the lift off length for 678 is significantly lower than for the other injector, which is coherent with its reduced mass flow rate.

Figure 34 displays the lift-off length as a function of ambient gas temperature for injector 678 and 677. Lift-off measurements of the nozzle 678 were performed at IFPEN in the two different vessels, whereas 677 measurements were performed at Sandia. The standard deviation is lower than ±2.6 mm for IFPEN results.

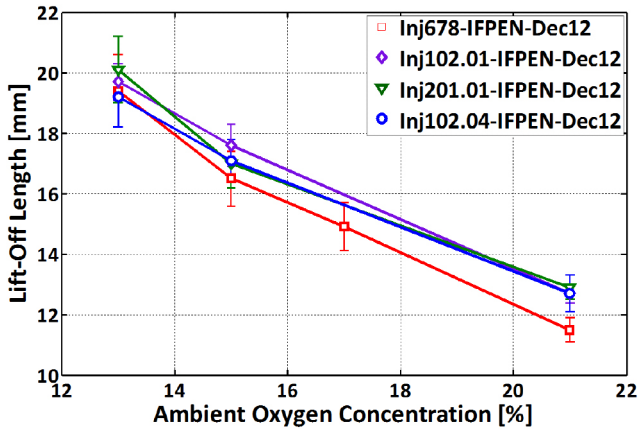

Figure 33. Effects of oxygen concentration on lift-off lengths for Spray A.2 and 678 injectors. Experimental conditions: 22.8kg/m^3, 900K, fuel at 373 K and 1500 bar injection pressure.

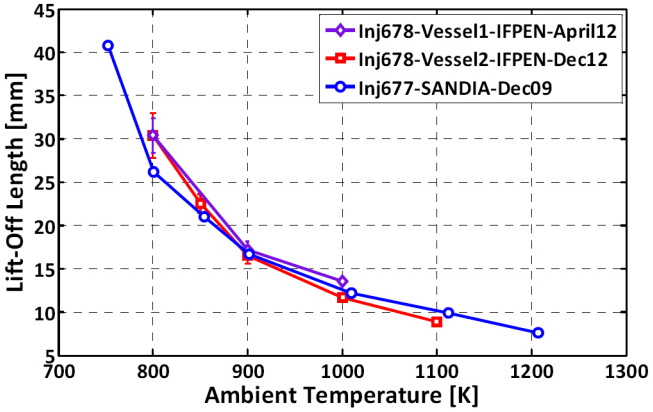

Figure 34. Effects of ambient temperature on lift-off lengths for ECN injectors at IFPEN and SANDIA. Experimental conditions: 22.8kg/m^3, 15% ambient oxygen, fuel at 373K and 1500 bar injection pressure.

The results show that the lift-off length of 678 obtained in the two IFPEN vessel are very similar and are in good agreement with the results of 677 obtained at Sandia. As expected ([20]), the ambient gas temperature has a strong effect on the lift-off length. The effect is non-linear, the sensitivity of lift-off length to ambient temperature decrease as the latter increases.

Figure 35 displays the lift-off length for three Spray A.2 injectors and compared to 678. Comparison of the lift-off length measurements for nozzles 102.01, 201.01 and 102.04 shows quite good agreement. Like for the oxygen concentration sweep, 678 shows slightly lower lift-off length than the Spray A.2 nozzles. At the targeted 900 K temperature, the variation span is around 1.1 mm, corresponding to 7%, which is lower than the standard deviation and also significantly lower than the dispersion obtained for the liquid length. This result shows that similarly

to vapor penetration and auto-ignition timing, the injector to injector variation has a much lower effect on lift off length than on liquid length.

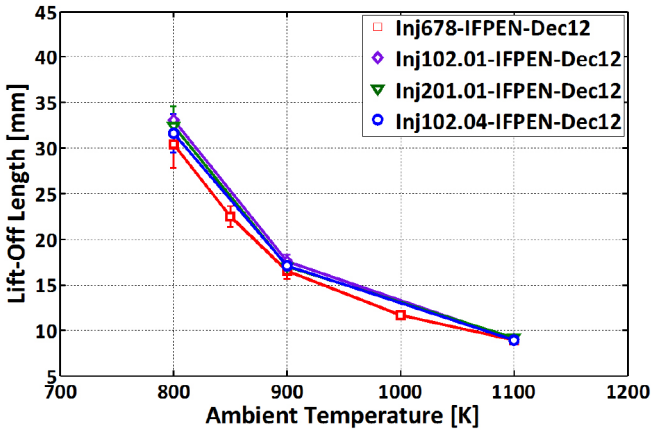

Figure 35. Effects of ambient temperature on lift-off lengths for Spray A.2 and 678 injectors. Experimental conditions: 22.8kg/m^3, 15% ambient oxygen, fuel at 373 K and 1500 bar injection pressure.

Similarly to the auto-ignition delay analysis, the tendencies of the evolution of the lift-off length against parameters sweep is analyzed thanks to a correlation formula. A scaling law has been defined in [20] to describe the effect of these parametric variations on the lift-off length:

$$H = C.T_a^a.\rho_a^b.U_0^c.d^d.Z_{st}^e \qquad (1.12)$$

where C is a constant, T_a [K] is the ambient gases temperature, ρ_a [kg/m^3] their density, U_0 [m/s] is the fuel velocity at the exit of the orifice, d [µm] is the orifice diameter and Z_{st} is the stoechiometric mixture fraction.

The experimental results obtained in the present work were compared with this law to the results obtained by other institutions, and the results are presented in Table 9.

Table 9. Comparison of the exponents used to fit experimental data with the scaling law given by (1.12)

	a	b	c	d	e
SAE 2005-01-3843	-3.74	-0.85	0.34	1	-1
Sandia (Inj 677 - Dec. 09)	-2.94	/	/	/	/
CMT (2nd ECN Workshop)	-3.89	-1	0.54	/	-1
IFPEN - Inj678 - Dec. 12	-3.82	/	/	/	-1.13
IFPEN – Inj102.01 - Dec. 12	-4.01	/	/	/	-0.97
IFPEN – Inj201.01 - Dec. 12	-3.86	/	/	/	-0.95
IFPEN – Inj102.04 - Dec. 12	-3.90	/	/	/	-0.91

Concerning the lift-off length dependence to ambient temperature, the results show that:

1. the dependence of lift-off length to temperature is in relatively good agreement with the scaling law. The a power dependence of the interpolated lines gives is −3.82 for injector 678, which is quite close to the value of −3.74 of the scaling law. Results obtained by CMT and presented at the 2nd ECN Workshop gave a value of −3.89.

2. this dependence is stronger at IFPEN with injector 678 than at Sandia with injector 677. Indeed, based on the interpolation, the lift-off length is proportional to T at the power −3.82 for IFPEN and power −2.94 for Sandia. This difference has not been further investigated at the moment.

3. Spray A.2 injectors show very similar results, with powers spanning between −3.86 and −4.00

Concerning the effect of oxygen concentration, the power dependence spans between −0.91 and −1.13, which is very close of the value of −1 proposed in the scaling law. This leads to the same conclusions than for the temperature variation: the behaviors of the different injectors are very similar, and in line with the scaling low.

In [20], a strong correlation was found between the auto-ignition delay and the lift-off length for different types of fuel and for various boundary conditions. The same correlation was therefore verified in the present work using the results obtained with the 678 and the Spray A.2 injectors 102.01, 201.02 and 102.04. This comparison is shown in Figure 36. For each condition four dots are plotted corresponding to the results obtained with the 4 different nozzles. The same global correlation between auto-ignition delays and lift off length is obtained in the present work, further confirming this correlation.

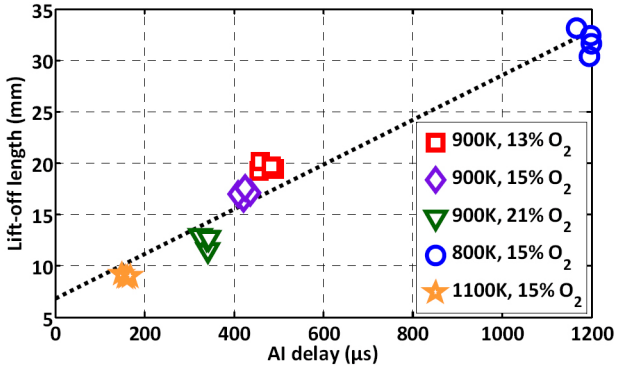

Figure 36. Comparison of the values of the lift-off length and the auto-ignition delay, for injectors 678, 102.01, 201.02 and 102.04.

SUMMARY/RECOMMENDATIONS

The characterization of 4 Spray A.2 injectors using standard ECN diagnostics has lead to of the following conclusions:

• Concerning the issue of boundary conditions control, it was found that small differences in vessel temperature control can affect significantly the final target conditions. In order to avoid any related uncertainty, a robust implantation system

for vessel temperature control is required. Following the present experiments, such a system has been designed at IFPEN in order to ensure similar operation between the two vessel.

• The targeting of the 2nd IFPEN constant volume vessel was reached at spray A boundary conditions, giving identical results in terms of spray characteristics between the two IFPEN vessels.

• Injector to injector comparison is best done with parameter sweeps since it provides a more robust analysis of the effect of boundary condition variations on spray characteristics.

• The behavior of Spray A.2 injectors has been investigated. The results show that all these injectors have very similar sprays characteristics, and are also very close to standard ECN injectors. This new set of injectors is therefore suitable for the ECN pool of injectors and are available to the community.

• This result shows that it is possible to include new injectors in the ECN pool in order to face the increasing number of participants, and also to face the issue of possible injector damage, if the latter are characterized as performed in the present study.

• However, differences in liquid length were observed between injectors that could not be explained by the nozzle diameter/mass flow rate information.

• These results tend to show that the analysis in the near field (at least up to the liquid tip location) requires a more detailed characterization, in particular of the internal geometry.

• However, it was found that the far field (vapor penetration, auto-ignition timing and lift off length) is less sensitive to differences between injectors, since very similar results were obtained.

Based on these conclusions, the following recommendations are proposed concerning the appropriate method to introduce new ECN injectors.

• Mass flow rates (and if possible momentum) characterizations and nozzle hole diameters determination should be performed prior to any spray characterization;

• Also, such characterizations should be performed after all experimental campaign to investigate potential aging effect;

• Standard ECN diagnostics should be performed with parameter sweeps around Spray A conditions in order to allow a robust comparison of the results against other injectors and institutions (in particular temperature and oxygen concentration since their variations are well characterized in the ECN database).

• In addition, internal geometry characterization should be performed to provide detailed information on the boundary conditions.

Finally, the following additional investigation could be performed in order to complement these conclusion:

• The same injector to injector comparisons could be carried out in another apparatus in order to verify if the same dispersion is observed;

• Momentum measurements of the Spray A.2 injectors would be interesting to complete the hydraulic characterization and possibly explain the differences obtained in the liquid length results;

• For the same reasons, internal geometry characterization would be of great interest, in particular if the Spray A.2 injectors were to be used for near field investigations.

REFERENCES

1. "http://www.sandia.gov/ecn/."
2. Pickett, L., Genzale, C., Bruneaux, G., Malbec, L. et al., "Comparison of Diesel Spray Combustion in Different High-Temperature, High-Pressure Facilities," *SAE Int. J. Engines* 3(2):156-181, 2010, doi: 10.4271/2010-01-2106.
3. Bardi M., Payri R., Malbec L.-M., Bruneaux G., Pickett L. M., Manin J., Bazyn T., and Genzale C., "Engine Combustion Network: Comparison Of Spray Development, Vaporization, And Combustion In Different Combustion Vessels," *Atomization and Sprays*, vol. 22 (10), pp. 807-842, 2012.
4. Meijer M., Somers B., Johnson J., Naber J., Lee S.-Y., Malbec L. M., Bruneaux G., Pickett L. M., Bardi M., Payri R., and Bazyn T., "Engine Combustion Network (Ecn): Characterization And Comparison Of Boundary Conditions For Different Combustion Vessels," *Atomization and Sprays*, vol. 22 (9), pp. 777-806, 2012.
5. Kastengren A. L., Tilocco F. Z., Powell C. F., Manin J., Pickett L. M., Payri R., and Bazyn T., "Engine Combustion Network (ECN): Measurements of Nozzle Geometry and Hydraulic Behavior," *Atomization and Sprays*, Submitted in 2012.
6. "1st ECN workshop, 13-14 May 2011, Ventura, California, http://www.sandia.gov/ecn/workshop/ECN1.php," 2011.
7. "2nd ECN workshop 7-8 Sept. 2012, Heidelberg, Germany, http://www.sandia.gov/ecn/workshop/ECN2.php," 2012.
8. Verhoeven, D., Vanhemelryck, J., and Baritaud, T., "Macroscopic and Ignition Characteristics of High-Pressure Sprays of Single-Component Fuels," SAE Technical Paper 981069, 1998, doi:10.4271/981069.
9. Meijer M., Malbec L.-M., Bruneaux G., and Somers L. M. T., "Engine Combustion Network: "Spray A" basic measurements and advanced diagnostics," *ICLASS* 2-6 Sept. 2012, Heidelberg, Germany, 2012.
10. Pickett L. M., Genzale C. L., Malbec J. M. L.-M., and Hermant L., "Measurement Uncertainty of Liquid Penetration in Evaporating Diesel Sprays," *ILASS Americas, 23rd Annual Conference on Liquid Atomization and Spray Systems*, 2011.
11. Gaydon A., *The Spectroscopy of Flames*. Chapman and Hall Ltd., London, 1974.
12. Higgins, B. and Siebers, D., "Measurement of the Flame Lift-Off Location on DI Diesel Sprays Using OH Chemiluminescence," SAE Technical Paper 2001-01-0918, 2001, doi:10.4271/2001-01-0918.
13. Siebers, D. and Higgins, B., "Flame Lift-Off on Direct-Injection Diesel Sprays Under Quiescent Conditions," SAE Technical Paper 2001-01-0530, 2001, doi:10.4271/2001-01-0530.
14. Cenker, E., Bruneaux, G., Pickett, L., and Schulz, C., "Study of Soot Formation and Oxidation in the Engine Combustion Network (ECN), Spray A: Effects of Ambient Temperature and Oxygen Concentration," *SAE Int. J. Engines* 6(1):352-365, 2013, doi:10.4271/2013-01-0901.
15. Naber, J. and Siebers, D., "Effects of Gas Density and Vaporization on Penetration and Dispersion of Diesel Sprays," SAE Technical Paper 960034, 1996, doi:10.4271/960034.
16. Siebers, D., "Liquid-Phase Fuel Penetration in Diesel Sprays," SAE Technical Paper 980809, 1998, doi:10.4271/980809.
17. Siebers, D., "Scaling Liquid-Phase Fuel Penetration in Diesel Sprays Based on Mixing-Limited Vaporization," SAE Technical Paper 1999-01-0528, 1999, doi:10.4271/1999-01-0528.
18. Pickett, L., Manin, J., Genzale, C., Siebers, D. et al., "Relationship Between Diesel Fuel Spray Vapor Penetration/Dispersion and Local Fuel Mixture Fraction," *SAE Int. J. Engines* 4(1):764-799, 2011, doi: 10.4271/2011-01-0686.
19. Siebers, D., Higgins, B., and Pickett, L., "Flame Lift-Off on Direct-Injection Diesel Fuel Jets: Oxygen Concentration Effects," SAE Technical Paper 2002-01-0890, 2002, doi:10.4271/2002-01-0890.

20. Pickett, L., Siebers, D., and Idicheria, C., "Relationship Between Ignition Processes and the Lift-Off Length of Diesel Fuel Jets," SAE Technical Paper 2005-01-3843, 2005, doi:10.4271/2005-01-3843.

ACKNOWLEDGMENTS

The technical expertise of Clement Bramoulle is greatly acknowledged. Also, Michele Bardi and Raul Payri from CMT are greatly acknowledged for their collaboration in performing and providing mass flow rate data. Julio C. C. Egúsquiza was financed by a postdoctoral fellowship from CNPq - Brazil.